Received June 9, 2019, accepted June 17, 2019, date of publication June 21, 2019, date of current version July 12, 2019.

Digital Object Identifier 10.1109/ACCESS.2019.2924178

Performance Analysis of MPSK FSO Communication Based on the Balanced Detector in a Fiber-Coupling System

HAIFENG YAO[1], XIAOLONG NI[1], CHUNYI CHEN[1], BO LI[1], XIANGLIAN FENG[2], XIANZHU LIU[1], ZHI LIU[1], SHOUFENG TONG[1], AND HUILIN JIANG[1]

[1]National and Local Joint Engineering Research Center of Space Optoelectronics Technology, Changchun University of Science and Technology, Changchun 130022, China

[2]State Key Laboratory of Modern Optical Instrumentation, Centre for Optical and Electromagnetic Research, Zhejiang University, Hangzhou 310058, China

Corresponding author: Shoufeng Tong (cust0888@163.com)

This work was supported in part by the National Natural Science Foundation of China under Grant 91438204, Grant 61475025, and Grant 61775022, in part by the Development Program of Science and Technology of Jilin Province of China under Grant 20180519012JH and Grant 20190201271JC, and in part by the Postdoctoral Science Foundation of China under Grant 2017M621179.

ABSTRACT An average bit error ratio (ABER) performance model for multiple phase shift keying (MPSK) based on a balanced detector with a fiber is presented in the free-space link for the first time. The Johnson S_B probability distribution function (pdf), to the best of our knowledge, is first experimentally explored, which can be used to describe the fading characteristics of an optical signal coupled into a single-mode fiber (SMF) in an atmospheric turbulence channel. Subsequently, an ABER expression is established by combining the photon characteristics of the balanced detector with the fiber. The numerical results show that the system has the most superior ABER performance when the splitting ratio is 0.5 and the quantum efficiency of the two photodetectors is equal. Moreover, the communication performances can be optimized by adjusting parameters, such as increasing the system bandwidth, selecting the appropriate modulation order, and improving the received optical power. Finally, the MPSK-signal-to-noise-ratio (SNR) model is also studied to evaluate system communication performance. Through our asymptotic analysis, if the required ABER falls below the 7% forward error correction (FEC) limit of 3.8×10^{-3}, the SNR should maintain at least 38 *dB* or more, while the normalized fluctuation variance deteriorates to 5.2441. This paper provides a parameter reference for designing the MPSK free-space optical (FSO) communication system, especially the fiber-coupling receiver.

INDEX TERMS Atmospheric modeling, optical fiber communication, optical transmitters, wireless communication.

I. INTRODUCTION

With the growing development of successfully achieving high-speed data transmission between the satellite and earth in many countries, free-space optical (FSO) communication has already shown the superiority of high bandwidth and no electromagnetic interference (EMI), and it has also pointed out the future development trend of high-speed communication [1], [2]. Compared to on-off-keying (OOK) and multi-level pulse amplitude modulation (MPAM), multiple phase shift keying (MPSK) has a better bit error rate (BER) performance under the same signal-noise ratio (SNR). In addition, MPSK can achieve the high-speed data transmission with 50 *GHz* channel spacing for improving high spectral utilization efficiency by using wavelength division multiplexing (WDM) system [3]–[6].

Currently, most of the experimental papers about the MPSK FSO communication system were demonstrated by using the fiber-coupling receiver system, e.g., see [7]–[10]. Our team also adopted this system to successfully demonstrate 40 *Gb/s* and 120 *Gb/s* differential phase shift keying (DPSK) FSO communication in 2017 and 2018, respectively [11]–[13]. These reports have a common feature, i.e., by using the lens, the free-space laser beam is

The associate editor coordinating the review of this manuscript and approving it for publication was San-Liang Lee.

coupled into the single mode fiber (SMF) such that the output light from the fiber can be directly focused on the effective receiving surface of the high-speed photodetector. However, most of the current theoretical works about MPSK FSO communication are based on lognormal, Gamma-Gamma, K distributed and other channel models, without further analysis of the instantaneous fading process of coupling the free-space optical signal into SMF after propagating through atmospheric turbulence [14], [15], such as the literature [16] derived the closed-form mathematical expressions for average bit error rate (ABER) estimation of radio on free-space optical (ROFSO) communication system by using Malaga distribution. W. Gappmair *et al*. demonstrated the FSO subcarrier PSK performance by employing Gamma-Gamma fading probability distribution function (PDF) [17]. In [18], Kiasaleh illustrated the BER performance based on the heterodyne FSO communication system by analyzing K distributed turbulence. In [19], Li *et al*. have analyzed the system performance of coherent detection spatial diversity based on Gamma-Gamma channel by coupling efficiency express. However, the PDF of the actual state is not given because the fiber received light intensity is instantaneously affected by channel variation in real time.

Furthermore, one of the most important parts of MPSK communication is the demodulation system. Although many documents have described the performance of the coherent demodulation system and the core device balance detector therein, the performance combined with the actual free-space channel model have not been discussed yet. The free-space channel is not as stable as the fiber channel because of the light intensity random fluctuation influenced by atmospheric turbulence [20]. Y. Wang *et al*. compared duobinary with differential phase-shift keying (DPSK) modulation by Monte Carlo simulation and investigated the balanced detection schemes in the fiber channel [21]. Y. Painchaud *et al*. theoretically and experimentally elaborated the performance of balanced detection in the coherent receiver system [22]. In [23], Leven *et al*. successfully demonstrated a signal processing method about coherent receiver at *GBaud* speed by adopting the fiber communication system. In theoretical terms, it is of great significance to establish a model of the MPSK FSO communication system in fiber-coupling and coherent detection for ABER statistics, and SNR performance analysis. In practical engineering, this model can as well as provide a reference for the design of the optical system and the selection of the device.

In this paper, by using the fiber-coupling FSO communication system, the ABER performance for MPSK mathematical model based on the balanced detector is first proposed. Section II introduces the Johnson S_B channel model for the fiber-coupling receiver system. Section III describes the ABER expression of MPSK based on the photon performance of the balanced detector by combining the Johnson S_B channel model. An experiment of Johnson S_B and numerical simulation of MPSK ABER performance are carried out, and an ABER-SNR model is established and analyzed, in Section IV. Finally, the conclusion is elaborated in Section V.

II. CHANNEL MODELS

The channel characteristics have been described by Gamma-Gamma, lognormal and other fading PDF in the FSO communication system [24, pp. 321-393]. If the fiber-coupling receiver system is employed, it means that SMF is used to receive the free-space optical signal in a coherent detection demodulation system, and output optical signal would be directly connected to a detector through SMF, as shown in Fig. 1.

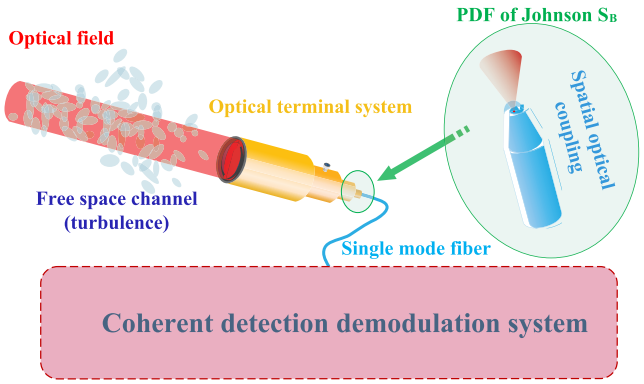

FIGURE 1. Schematic diagram of coupling spatial optical signal into SMF.

These PDFs are not suitable for depicting the optical signal fading characteristics. Because instantaneous optical signal fading at the SMF is essentially determined by the light field at the front end of the SMF, the atmosphere turbulence strength and the square magnitude of coupling coefficient. In order to better portray this phenomenon, we presented the Johnson S_B model in our previous work, and demonstrated the suitability of Johnson S_B from strong to weak turbulence in the process of coupling free-space light into SMF through numerical simulation [25, Sec. 3]. Hence, this work utilizes the Johnson S_B PDF to illustrate channel fading characteristics, and the normalized form is given by

$$p(\zeta)=\frac{\delta}{\sqrt{2\pi}}\frac{1}{\zeta(1-\zeta)}\exp\left\{-\frac{1}{2}\left[\gamma+\delta\ln(\frac{\zeta}{1-\zeta})\right]^2\right\}. \quad (1)$$

The ζ is normalized light intensity which obeys $0<\zeta<1$. δ and γ are free parameters which can be calculated by average light intensity $E(\zeta)$ and light intensity fluctuation variance σ_ζ^2, as follows

$$E(\zeta)=\left\langle\zeta^1\right\rangle, \quad (2)$$

$$\sigma_\zeta^2=\left\langle\zeta^2\right\rangle-\left\langle\zeta^1\right\rangle^2, \quad (3)$$

where the $\langle\zeta^n\rangle=\int_0^1\zeta^n p(\zeta)d\zeta$ is the n^{th} moment. In actual engineering, the absolute light intensity values χ can be expressed as

$$p_{JSB}(\chi)=p(\zeta\cdot\zeta_{optimal}), \quad (4)$$

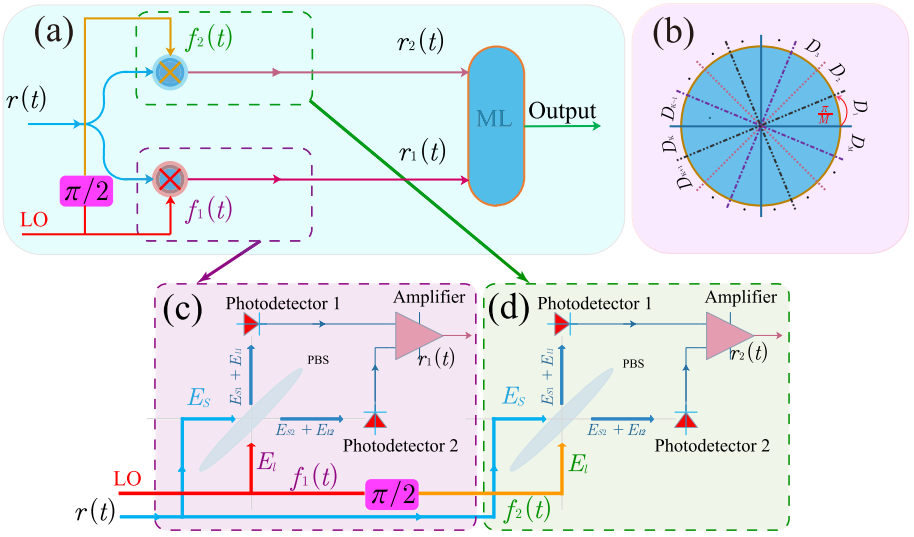

FIGURE 2. Coherent detection demodulation system. (a) The schematic diagram of coherent demodulation. (b) The optimal phase decision of coherent demodulation. (c) The schematic diagram of coherent demodulation for balanced detection, where the PBS is polarization beam splitter, LO optical signal is f_1. (d) The LO optical signal is f_2 which is $\pi/2$ out of phase with f_1, its optical system is the same as (c).

where $\zeta_{optimal}$ represents the optimum light intensity coupled into the SMF, and $\chi = \zeta \cdot \zeta_{optimal}$ is the received instantaneous light intensity.

III. MPSK MODEL BASED ON BALANCED DETECTOR

Assuming that the dispersion of the fiber is not considered and the light field after polarization controller (PC) is within the detectable range, the received optical signal in the SMF of Fig. 2 can be expressed as

$$r(t) = s_i(t) + n(t), \tag{5}$$

here $s_i(t)$ is the MPSK optical signal which can be written as

$$s_i(t) = E_s \cos(2\pi f_s t + \frac{2\pi(i-1)}{M}) \begin{cases} 0 \le t \le T_s \\ i = 1, 2, \cdots, M, \end{cases} \tag{6}$$

$$ENG = \int_0^{T_s} s_i^2(t)dt = \frac{1}{2} I_s = \frac{1}{2} E_s^2. \tag{7}$$

where E_s, ENG and I_s represent the amplitude, the energy in T_s, and the SMF received optical signal power, respectively. In addition, $T_s = (\log_2 M)T_b$, T_s is the M-ary symbol interval, and T_b is the binary optical signal interval. f_s denotes the optical signal frequency. $\varphi_s = 2\pi(i-1)/M$ represents the modulated phase. $n(t)$ indicates the additive white Gaussian noise (AWGN) which is generated by the detector during which photons are converted to the photocurrent. By performing orthogonal decomposition for (6), it can be expressed as [26, pp. 643-645]

$$\begin{aligned} s_i(t) &= s_{i1}(t)f_1(t) + s_{i2}(t)f_2(t) \\ &= \sqrt{ENG}[a_{i1}f_1(t) + a_{i2}f_2(t)], \end{aligned} \tag{8}$$

here, $f_1(t) = \sqrt{2/T_s}\cos(2\pi f_s t)$ and $f_2(t) = -\sqrt{2/T_s}\sin(2\pi f_s t)$ denote an orthogonal base signal, where (8) exists $a_{i1}^2 + a_{i2}^2 = 1$, $a_{i1} = \cos(2\pi/(i-1))$ and $a_{i2} = \sin(2\pi/(i-1))$. Thus, $r_i(t)$ can be written as a two-dimensional vector signal, there is

$$\overrightarrow{r_i} = [r_1, r_2]. \tag{9}$$

Under maximum likelihood (ML) criterion, the MPSK optical signal waveforms have equal probability, this schematic is depicted in Figs. 2(a) and (b). We perform coordinate transformation on r_1 and r_2, the detected optimal vector phase θ_r can be expressed as [27, pp. 21-25]

$$\theta_r = \arctan\frac{r_2}{r_1}. \tag{10}$$

The MPSK optical signals can be demodulated by dividing different receiving domains. In this case, we can calculate the optimal ABER. First, we shall assume that the transmitted optical signal is $s_i(t)$ which is represented by the following vector

$$s_1 = [\sqrt{ENG}, 0]. \tag{11}$$

Meanwhile, assuming that $r_1 = \sqrt{ENG} + n_1$ and $r_2 = n_2$. Since we previously assumed that the noise is AWGN, r_1 and r_2 are joint Gaussian distributions, that is, we can get the received optical signal mean $E(r_1|s_1)$, $E(r_2|s_1)$ and the received optical signal variance $D(r_1|s_1)$, $D(r_2|s_1)$, which are given by

$$E(r_1|s_1) = \sqrt{ENG}, \qquad E(r_2|s_1) = 0, \tag{12}$$

$$D(r_1|s_1) = D(r_2|s_1) = \sigma_{balance}^2. \tag{13}$$

Considering the model of actual coherent demodulation, it needs a strong local oscillator (LO) optical signal and a photodetector which cannot be directly demodulated like radio frequency (RF) [22], [28]–[30]. It is extremely necessary for

us to analyze the received MPSK optical signal. In actual engineering, the balanced detector is often utilized to detect and demodulate the MPSK optical signal, which can improve the SNR. Therefore, the LO optical signals can be rewritten as $f_1(t) = E_l \cos(2\pi f_l t + \varphi_l)$, $f_2(t) = E_l \sin(2\pi f_l t + \varphi_l)$. We only discuss one of two balanced detectors because their structures are the same, which are shown in Figs. 2(c) and (d). By observing the structure of the balanced detector, we note that the photocurrent i_1, i_2 of photodetector is generated after absorbing the coupler output optical signal. Hence, within each bit of information, the i_1 and i_2 can be expressed as [22, Eqs. (8)-(24)]

$$i_1 = \frac{\eta_1 q}{h\nu}\{(1-\varepsilon)E_s^2 + \varepsilon E_l^2 - 2\sqrt{1-\varepsilon}\sqrt{\varepsilon} \times E_s E_l \sin[(2\pi f_s - 2\pi f_l)t + (\varphi_s - \varphi_l)]\} + n_{11}, \quad (14)$$

$$i_2 = \frac{\eta_2 q}{h\nu}\{\varepsilon E_s^2 + (1-\varepsilon)E_l^2 + 2\sqrt{1-\varepsilon}\sqrt{\varepsilon} \times E_s E_l \sin[(2\pi f_s - 2\pi f_l)t + (\varphi_s - \varphi_l)]\} + n_{12}, \quad (15)$$

where $E_l = \sqrt{I_l}$, f_l, φ_l, and I_l represent the amplitude, frequency, phase and optical power of the LO, respectively. η_1, η_2 represent quantum efficiency, ε is the splitting ratio of the coupler, and n_{11}, n_{12} denote the current noise of the photodetector. Moreover, h is Planck's constant and q is the electron charge. $\nu = c/\lambda$ denotes the optical frequency, c and λ are optical velocity and wavelength. According to the structure of differential amplifier circuit (see, Fig. 2(c)), we can get

$$i_2 - i_1 = \frac{q}{h\nu}\{[\varepsilon\eta_2 - (1-\varepsilon)\eta_1]E_s^2 + [(1-\varepsilon)\eta_2 - \varepsilon\eta_1]E_l^2\} + \frac{q}{h\nu}\{2(\eta_1+\eta_2)\sqrt{1-\varepsilon}\sqrt{\varepsilon}E_s E_l \times \sin[(2\pi f_s - 2\pi f_l)t + (\varphi_s - \varphi_l)]\} + \{n_{12} - n_{11}\}. \quad (16)$$

The intermediate frequency signal $i_{balance1}$ and the amplitude $\langle i_{balance}\rangle$ can be obtained by filter and amplifier, here the G is amplifier gain.

$$i_{balance1} = G\frac{q}{h\nu}\{2(\eta_1+\eta_2)\sqrt{1-\varepsilon}\sqrt{\varepsilon}E_s E_l \times \sin[(2\pi f_s - 2\pi f_l)t + (\varphi_s - \varphi_l)]\} + n_1, \quad (17)$$

$$\langle i_{balance}\rangle = G\frac{q}{h\nu}\{2(\eta_1+\eta_2)\sqrt{1-\varepsilon}\sqrt{\varepsilon}E_s E_l. \quad (18)$$

Therefore, the $r_1(t)$ can be written as

$$r_1(t) = \langle i_{balance}\rangle \sin[(2\pi f_s - 2\pi f_l)t + (\varphi_s - \varphi_l)] + n_1. \quad (19)$$

where the n_1 and n_2 are the total noise of the two balanced detectors respectively. Similar, we can get

$$r_2(t) = \langle i_{balance}\rangle \cos[(2\pi f_s - 2\pi f_l)t + (\varphi_s - \varphi_l)] + n_2. \quad (20)$$

Especially, when $f_s = f_l$, this is homodyne detection, Otherwise this is heterodyne detection [22]. Assuming that the balance detector is a PIN photodiode, the total noise (n_1 or n_2) contains noise, shot noise, and thermal noise of the output current. Wherein, the excess noise is caused by the optical power random fluctuation due to the jitter of the LO optical signal. The mean value relationship between relative intensity noise (RIN) and the mean square of noise power $\langle I_N^2\rangle$ is given in [31, pp. 221], as follows

$$RIN = 10\log_{10}\frac{\langle I_N^2\rangle}{\langle I_l\rangle^2 B}. \quad (21)$$

Therefore, the expression of the square of excess noise current can be derived

$$\sigma^2_{excess-balance} = 2q\xi(G\frac{q}{h\nu})^2[\eta_1\varepsilon E_l^2 - \eta_2(1-\varepsilon)E_l^2]^2 B, \quad (22)$$

where $\xi = (10^{RIN/10})/(2q)$ denotes the variation of the LO optical signal noise power with the square of average LO optical power, B represents the bandwidth of the detector and $B = 1/2\,T_s$ [22, Eq, (35)]. Additionally, the shot noise is incoherent noise, which is given by [32, pp. 501-538]

$$\sigma^2_{shot-balance1} = 2qG^2[i_1 + i_{d1}]B, \quad (23)$$

$$\sigma^2_{shot-balance2} = 2qG^2[i_2 + i_{d2}]B, \quad (24)$$

where $\sigma^2_{shot-balance1}$ and $\sigma^2_{shot-balance2}$ denote the short noise of two PINs, respectively. i_{d1} and i_{d2} are the dark current noise of the two PINs. We shall assume the system uses an optical filter that can filter out the background noise, consequently, the noise is not considered here. We also know that the temperature characteristics of the balanced detector can cause thermal noise $\sigma^2_{thermal-balance} = 4\kappa TB/R$, where the parameters are *Kelvin* temperature constant κ, the device temperature T and the load impedance R. $\sigma^2_{thermal-balance}$ is the noise of the balance detector itself, which is determined by the device temperature, the load impedance and bandwidth, and does not vary with the gain of the amplifier [32, Sec. 10.5]. It is noteworthy that the photoelectric conversion of the detector is a Poisson process. When the number of the photons absorbed by the detector surface is much greater than 1, this can be approximated as a Gaussian distribution [20, pp. 225-230]. In this paper, the balance detector has a LO optical signal, i.e., the number of photons is much greater than 1. In MPSK signal, we also discover that the $ENG = \frac{1}{2}\log_2 M\langle i_{balance}\rangle^2$ [32]. Hence, (12) and (13) can be written as

$$E(r_1|s_1) = \sqrt{\frac{1}{2}\log_2 M\langle i_{balance}\rangle^2} \qquad E(r_2|s_1) = 0, \quad (25)$$

$$D(r_1|s_1) = D(r_2|s_1) \approx \sigma^2_{excess-balance} + \sigma^2_{shot-balance1} + \sigma^2_{thermal-balance}, \quad (26)$$

$$\approx \sigma^2_{excess-balance} + \sigma^2_{shot-balance2} + \sigma^2_{thermal-balance}, \quad (27)$$

According to (9), (25) and (26), the joint conditional PDF can be given by

$$p(r_1 r_2|s_1) = \frac{1}{2\pi\sigma^2_{balance}} \times \exp\{\frac{r_1 + \sqrt{\frac{1}{2}\log_2 M \langle i_{balance}\rangle^2}}{2\sigma^2_{balance}} - \frac{r_2}{2\sigma^2_{balance}}\}. \quad (28)$$

Simultaneously, we can also get

$$p(\theta_r|s_1) = \sqrt{\log_2 M \frac{\langle i_{balance}\rangle^2}{2\pi\sigma^2_{balance}}}\cos\theta_r \times \exp(-\log_2 M \frac{\langle i_{balance}\rangle^2}{2\sigma^2_{balance}}\sin^2\theta_r). \quad (29)$$

According to [26, pp. 644], the average symbol error rate (ASER) is given by

$$P_{SER-balance} = 2Q(\sqrt{\log_2 M \frac{\langle i_{balance}\rangle^2}{\sigma^2_{balance}}}\sin\frac{\pi}{M}). \quad (30)$$

Thus, the ABER based on balanced detector without atmospheric turbulence can be written as

$$P_{ABER-balance} = \frac{1}{\log_2 M}P_{SER-balance} = \frac{2}{\log_2 M}Q(\sqrt{\log_2 M \frac{\langle i_{balance}\rangle^2}{\sigma^2_{balance}}}\sin\frac{\pi}{M}). \quad (31)$$

Considering the fiber-coupling, the final joint ABER analytical expression is given by

$$P_{ABER} = \int_0^\infty p_{JSB}(\zeta)P_{ABER-balance}d\zeta. \quad (32)$$

In [20, pp. 226, Eqs. 5-8], we know that the number of photons absorbed by the photodetector effective area A_d can be written as

$$K_n = \frac{\eta}{h\nu}\int_0^{T_s} I_s(t)dt = \frac{\eta}{h\nu}\int_0^{T_s} A_d\zeta(t)dt. \quad (33)$$

According to (33), the (32) can be written as

$$P_{ABER} = \int_0^\infty \frac{2}{\log_2 M}\frac{\delta}{\sqrt{2\pi}}\frac{I_{soptimal}}{I_s(I_{soptimal}-I_s)} \times \exp\left\{-\frac{1}{2}\left[\gamma + \delta\ln(\frac{I_s}{I_{soptimal}-I_s})\right]^2\right\} \times Q(\sqrt{\log_2 M \frac{\langle i_{balance}\rangle^2}{\sigma^2_{balance}}}\sin\frac{\pi}{M})dI_s. \quad (34)$$

It is worth noting that $\langle i_{balance}\rangle^2/\left(2\sigma^2_{balance}\right)$ is the SNR of balanced detector, where $2\sigma^2_{balance}$ is the sum of the noise powers of two PINs. Hence, SNR can be written as

$$SNR(I_s) = \frac{\langle i_{balance}\rangle^2}{2\sigma^2_{balance}} = 2\left(\frac{q}{h\nu}\right)^2 G^2(\eta_1+\eta_2)^2\varepsilon(1-\varepsilon)I_l I_s \times \left[\begin{array}{l} 2q\xi(G\frac{q}{h\nu})^2[\eta_1\varepsilon-\eta_2(1-\varepsilon)]I_l^2 B+ \\ qG^2\left[\begin{array}{l}\frac{q}{h\nu}[\eta_1\varepsilon+\eta_2(1-\varepsilon)]I_l \\ +i_{d1}+i_{d2}\end{array}\right]B+ \\ \frac{4\kappa TB}{R}\end{array}\right]^{-1} \quad (35)$$

Equation (34) is a general analytical expression. It indicates that statistical calculations can be implemented to analyze the MPSK ABER performance in the fiber-coupling receiver system using the average received power as a test variable. Here $I_{soptimal}$ is the optimal received optical power from the SMF. Compared to the already reported ABER expression without the beam splitting ratio (e.g., [6], [18], [22]), (34) is an ABER expression about the photoelectric performance of balanced detector. By analyzing (34) and (35), we can better draw a conclusion that the ABER performance is affected by turbulence strength, optical power, gain, splitting ratio, quantum efficiency, bandwidth, temperature, etc.

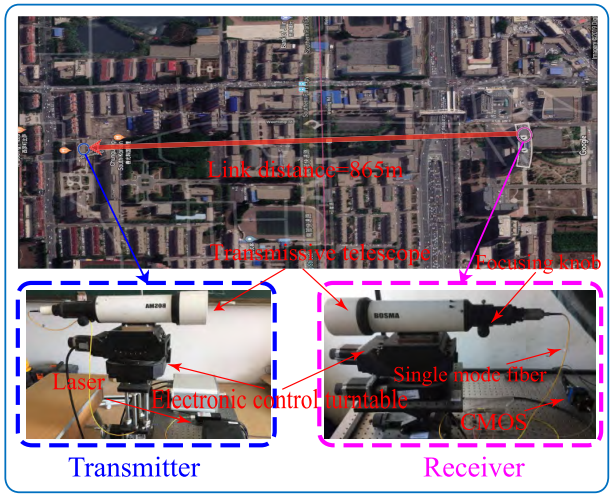

FIGURE 3. Light intensity fading measurement system. The link distance = 865 *m*, the laser wavelength = 1550 *nm*, the optical power = 27 *dBm* (500 *mW*), the optical system structure at the transmitter is the same as the receiver, the alignment system is electronically controlled turntable, the detector is CMOS which receive the light intensity from SMF.

IV. NUMERICAL ANALYSIS

From the beginning, we performed a three-month experimental verification for the Johnson S_B channel model (July 2018 to October 2018), as shown in Fig. 3. In order to eliminate the interference of background light, the experiment was carried out at 20:00-22:30. The experimental site

was located at Changchun University of Science and Technology, with a link distance of 865 m. The transmitter used a transmissive telescope with adjustable focal length and 100 mm aperture diameter, a 26.9 dBm (500 mW) laser source of 1550 nm, and alignment system composed of the electronically controlled turntable. The optical system at the receiver has the same structure as the transmitter, which can couple light into the SMF by adjusting the focal length. The complementary metal oxide semiconductor (CMOS, CAMMC1362) was employed to detect the light intensity from the fiber, and the sampling frequency is 1 kHz. Through measurement, we discovered that if the light is completely received by transmissive telescope and not coupled into the fiber, the received optical power is about 25.7 dBm (380 mW), it means the system without fiber coupling has about -11.9 dB attenuation in 865 m atmospheric turbulence channel.

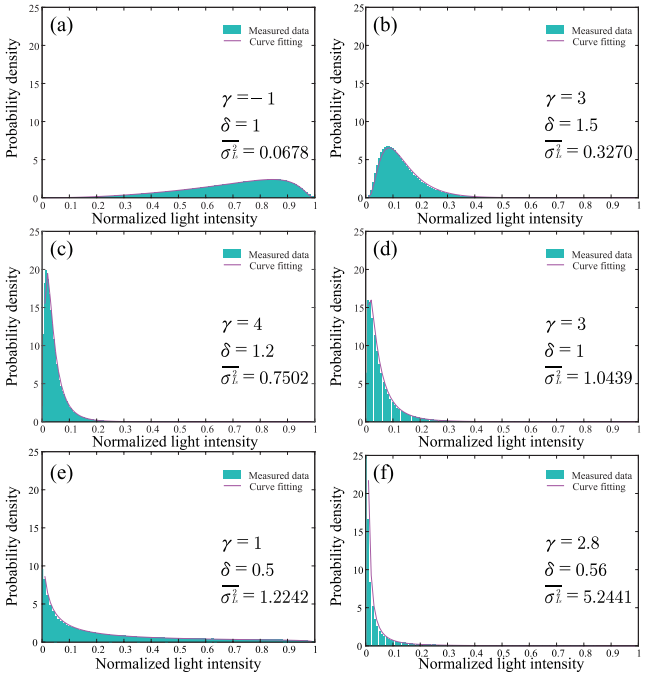

FIGURE 4. Experimental verification of Johnson S_B. (a)-(f) Measured atmospheric conditions are $C_n^2 = 1.1 \times 10^{-16}\ m^{-2/3}$, $C_n^2 = 5.5 \times 10^{-16}\ m^{-2/3}$, $C_n^2 = 1.3 \times 10^{-15}\ m^{-2/3}$, $C_n^2 = 1.7 \times 10^{-13}\ m^{-2/3}$, $C_n^2 = 2.1 \times 10^{-13}\ m^{-2/3}$ and $C_n^2 = 8.9 \times 10^{-13}\ m^{-2/3}$ respectively; the fitting efficiencies are 0.9996, 0.9657, 0.9791, 0.9457, 0.9967, and 0.9454 respectively.

Subsequently, for ease of analysis, assume that dispersion is not considered here. According to (1), we performed off-line analysis of the sampled data, where the fading profile and the fit curve are as depicted in Fig. 4. Meanwhile, it is worth noting that the normalized fluctuation variance is defined as

$$\overline{\sigma_{I_s}^2} = \frac{\langle {I_s}^2 \rangle - \langle {I_s}^1 \rangle^2}{\langle {I_s}^1 \rangle^2}. \tag{36}$$

It can be seen that, as the curve moves closer to the ordinate, the normalized variance will be larger. It indicates that the channel is highly deteriorated. The measured atmospheric conditions of Figs. 4(a)-(f) are $C_n^2 = 1.1 \times 10^{-16}\ m^{-2/3}$, $C_n^2 = 5.5 \times 10^{-16}\ m^{-2/3}$, $C_n^2 = 1.3 \times 10^{-15}\ m^{-2/3}$, $C_n^2 = 1.7 \times 10^{-13}\ m^{-2/3}$, $C_n^2 = 2.1 \times 10^{-13}\ m^{-2/3}$ and $C_n^2 = 8.9 \times 10^{-13}\ m^{-2/3}$ respectively. And the fitting efficiencies are 0.9996, 0.9657, 0.9791, 0.9457, 0.9967, and 0.9454 respectively. It can be concluded that when the light beam passes through "weak, moderate and strong" turbulence, Johnson S_B PDF can describe the optical signal distribution state. Its performance is better than other models such as Lognormal and Gamma-Gamma.

Secondly, because the receiving end is a SMF, its effect on the optical wave is equivalent to filtering in spatial domain. The wavefront is distorted while the optical signal is propagating in the atmospheric channel, the existing channel models are not suitable for describing the channel state at this time. From an engineering point of view, the channel parameters can be determined by actually testing their mean and variance, which is beneficial to the estimation of the channel PDF. Based on the above experimental results, we use Johnson S_B PDF to express the channel state of the fiber-coupled system in FSO communication. In particular, in the following section, we use the fitted parameters of Johnson S_B to simulate.

By observing (35), the SNR of the balanced detector has an important influence on the ABER. If splitting ratio is just adapted, i.e., $\varepsilon = 0.5$, the SNR of balanced detector has a maximum value, which shows that the balance detector possesses the optimal performance, as depicted in Fig. 5(a), where the simulation parameters are set to $\lambda = 1550\ nm$, $\xi = 1.0 \times 10^5$, $G = 200$, $T = 300\ K$, $R = 50\ \Omega$, $B = 4\ GHz$, $symbol\ rate = 2\ GB/s$, $i_{d1} = i_{d2} = 1.0 \times 10^{-9}\ nA$. When the input LO optical power is 13.9794 dBm (25 mW), the input MPSK optical power is -12.412 dBm (0.0625 mW) and the splitting ratio is 0.5, the SNR of balanced detector up to 56.4221 dB which is higher than $\varepsilon = 0.3$ (or 0.7) by 26 dB. Therefore, the splitting ratio is set to $\varepsilon = 0.5$. Furthermore, we know that the input MPSK optical power I_s is one of the key factors affecting detection performance. As the MPSK optical power increases, the SNR of the balanced detector raises. The SNR of -40 dBm MPSK optical power is 10 dB more than the -50 dBm if the splitting ratio is 0.5 and the LO optical power is 13.9794 dBm. In this numerical experiment, the following scenarios of MPSK optical power from -50 dBm to -30 dBm are highlighted for better exploring the ABER performance under minimum received optical power.

Compared to Fig. 5(a), Fig. 5(b) depicts the SNR performance of the balanced detector under the different quantum efficiency of PIN photodetectors. The SNR of balanced detector is optimal which reaches a maximum value 18.9209 dB ($I_l = 13.9794\ dBm$, $I_s = -50\ dBm$) when $\eta_1 = \eta_2 = 1$. The ABER performance is presented by the contour line, which is shown in Fig. 6. The excess noise can be eliminated in the event that the two PIN photodetectors have the best same process level and the coupler has the best splitting ratio performance, i.e., if $\eta_1 = \eta_2$ and $\varepsilon = 0.5$, then $\sigma^2_{excess-balance} = 0$. The ABER is the lowest in the case of that the quantum

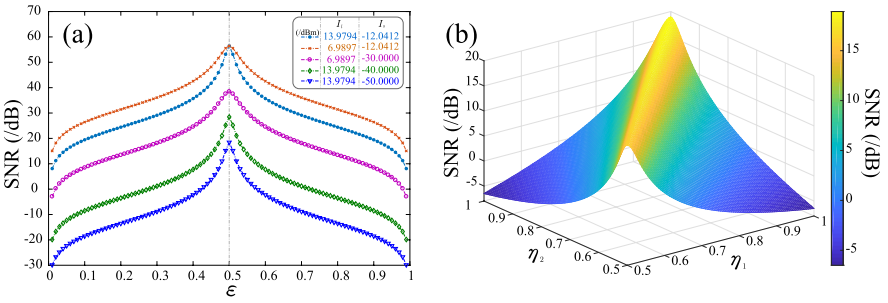

FIGURE 5. SNR performance of balance detector for splitting ratio ε and quantum efficiency η_1, η_2 of two PIN photodetectors. The common parameter $\lambda = 1550$ *nm*, $\xi = 1.0 \times 10^5$, $G = 200$, $T = 300$ *K*, $R = 50\ \Omega$, $B = 4$ *GHz*, *symbol rate* $= 2$ *GB/s*, $i_{d1} = i_{d2} = 1.0 \times 10^{-9}$ *nA*; (a) ε, I_l and I_s are variables, $\eta_1 = \eta_2 = 0.9$; (b) η_1 and η_2 are variables, $\varepsilon = 0.5$, $I_l = 25$ *dBm*, $I_s = -50$ *dBm*.

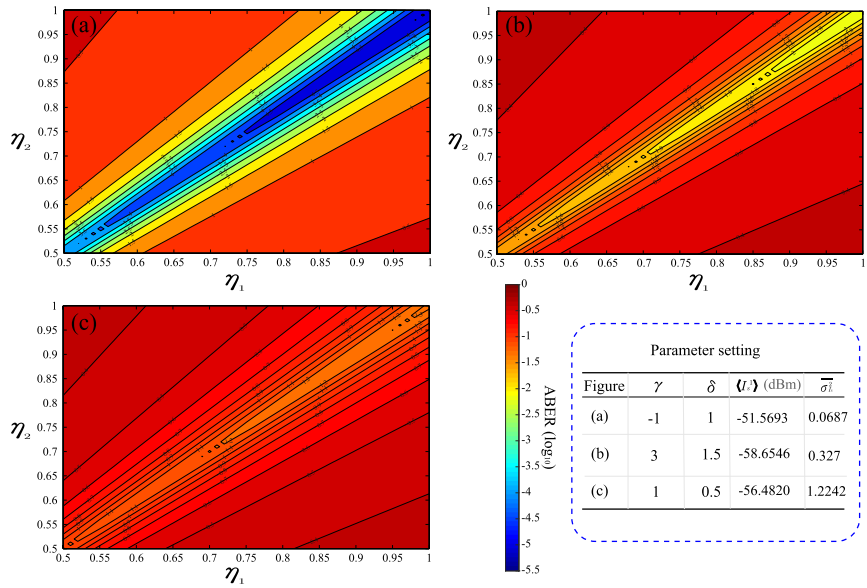

FIGURE 6. ABER as a function of quantum efficiency η_1 and η_2 of two PIN photodetectors for MPSK. $M = 4$, $\lambda = 1550$ *nm*, $\varepsilon = 0.5$, $\xi = 1.0 \times 10^5$, $G = 200$, $T = 300$ *K*, $R = 50\ \Omega$, $B = 4$ *GHz*, *symbol rate* $= 2$ *GB/s*, $i_{d1} = i_{d2} = 1.0 \times 10^{-9}$ *nA*, $I_l = 3.9794$ *dBm*, $I_{soptimal} = -50$ *dBm*. (a), (b) and (c) represent $\gamma = -1, 3, 1$; $\delta = 1, 1.5, 0.5$, respectively.

efficiency tends to the ideal state, i.e, $\eta_1 \to 1$ and $\eta_2 \to 1$, the system will get an optimum SNR. Hence, considering the strict consistency requirements of balance detector, we shall set the parameters $\eta_1 = \eta_2 = 0.9$ in the following simulation. We then found that the ABER increases with the increase of the $\sigma_{I_s}^2$, it means that the ABER will deteriorate rapidly while the turbulence strength enhances. The ABER has a significant deterioration trend when $\sigma_{I_s}^2$ changes from 0 to 0.1, as described in Fig. 6 (a) and (b). For example, Fig. 6 (a) ($ABER = 1.3518 \times 10^{-5}$) is two orders of magnitude lower than Fig. 6 (b) ($ABER = 8.6520 \times 10^{-3}$) when the quantum efficiency is 0.9, the LO optical power is 13.9794 *dBm* and the MPSK optical power is -50 *dBm*. As the turbulence strength increases, the optimal ABER becomes to 5.20×10^{-2} below the 7% forward error correction (FEC) limit of 3.8×10^{-3}, as shown in Fig. 6(c) [33].

Furthermore, the ABER performance of different modulation order M under the different atmospheric channels was explored, as presented in Fig. 7. The ABER increases with the deterioration of channel quality when the modulation order is the same. It is worth noting that under the same free-space channel environment and transmission power, as the order of M decreases, the communication quality is gradually improved. This can verify the existing literature [8], [11], which have successfully achieved the high-rate FSO communication by using BPSK or DPSK. For a better discussion here, the numerical experiment was carried out based on $M = 4$ in the following pages. Besides, improving the received power of the SMF can further enhance the communication performance. For instance, the ABER at the received power of -25 *dBm* is 5 orders of magnitude lower than the -50 *dBm* when $\gamma = 3.2$, $\delta = 1$ and $M = 4$, as shown in Fig. 7(b). That is the reason we used the optical terminal system to improve the received power of SMF in our previous work [11].

However, the balanced detector has a maximum damage optical power threshold, i.e., maximum input optical power limit. On this basis, we found that the gain and temperature of the balance detector are also an important factor affecting

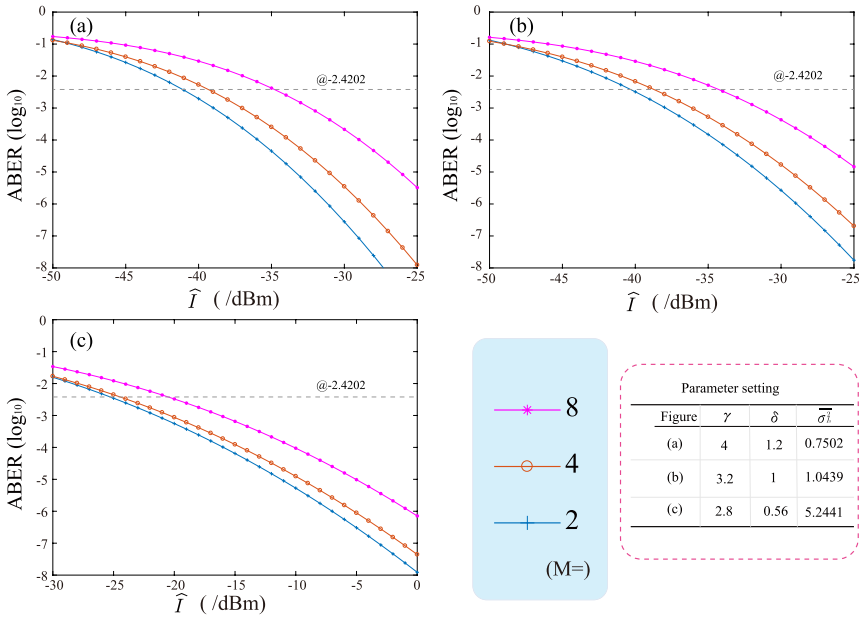

FIGURE 7. ABER as a function of modulation order M for MPSK. @-2.4202 denotes 3.8×10^{-3} ABER, $\eta_1 = \eta_2 = 0.9$, $\lambda = 1550$ *nm*, $\varepsilon = 0.5$, $\xi = 1.0 \times 10^5$, $G = 200$, $T = 300$ *K*, $R = 50\ \Omega$, $B = 4$ *GHz*, *symbol rate* $= 2$ *GB/s*, $i_{d1} = i_{d2} = 1.0 \times 10^{-9}$ *nA*, $I_l = 3.9794$ *dBm*. (a), (b) and (c) represent $\gamma = 4, 3.2, 2.8$; $\delta = 1.2, 1, 0.56$, respectively.

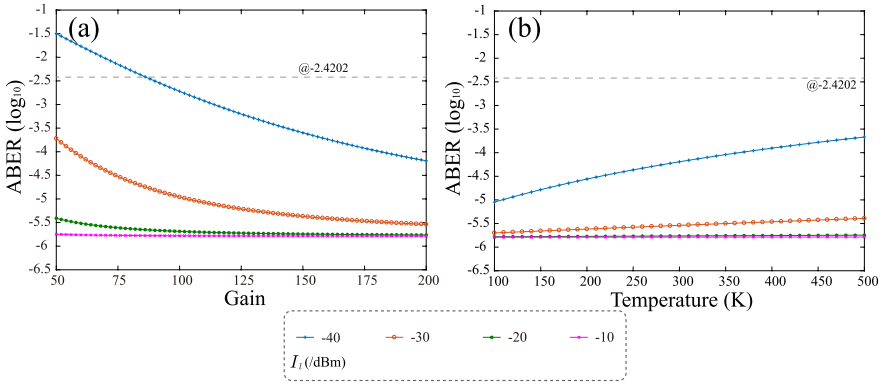

FIGURE 8. ABER as a function of balanced detector gain G and temperature T for MPSK. @-2.4202 denotes 3.8×10^{-3} ABER, the common parameter $M = 4$, $\eta_1 = \eta_2 = 0.9$, $\lambda = 1550$ *nm*, $\varepsilon = 0.5$, $\xi = 1.0 \times 10^5$, $R = 50\ \Omega$, $B = 4$ *GHz*, *symbol rate* $= 2$ *GB/s*, $i_{d1} = i_{d2} = 1.0 \times 10^{-9}$ *nA*, $I_{soptimal} = -40$ *dBm*, $\gamma = 3$, $\delta = 1.5$; (a) G is a variable, $T = 300$ *K*; (b) T is a variable, $G = 200$.

detection performance under low input optical power (see, Eq. (35)). Therefore, we explored the ABER performance among different gain, temperature, and LO optical power under the atmospheric channel $\sigma_{I_s}^2 = 0.327$, as shown in Figs. 8(a) and (b). When the LO optical power lower is less than -30 *dBm*, the ABER performance is ameliorated with the higher gain G or the lower temperature K. Nevertheless, it indicates that the ABER tends to be stable when the LO optical power is greater than -10 *dBm* and reflects signal distortion effect has weakened. According to this relationship, we can design the temperature control system to keep a good working state and prevent the detector from burning out for better stabilizing the optical-electrical conversion performance of the balance detector. Moreover, we can design a high gain amplifier to make output signal from the balance detector meet the processing range of the digital signal circuit.

It cannot be ignored that the atmosphere channel can be regarded as a filter, and the envelope of the fading PDF can be affected by wavelength and frequency [24, pp. 152-154]. To investigate this effect, three different channel environments were assumed, i.e., $\gamma = 4$, $\delta = 1.2$; $\gamma = 3.2$, $\delta = 1.5$ and $\gamma = 1$, $\delta = 0.5$ as shown in Figs. 9 and 10. Under the same received power of SMF, we chose a longer wavelength optical signal, which is beneficial to moderate the ABER. However, as the degree of turbulence intensity increases, the communication quality deteriorates. Especially, the ABER is higher than the 7% FEC limit of 3.8×10^{-3}(@ $-$ 2.4202) when the channel parameters are $\gamma = 1$, $\delta = 0.5$, the received signal power is -35 *dBm* and the wavelength is less than 800 *nm*. It shows that communication failed under such conditions, as described in Fig. 9(b). The ABER can be also decreased by reducing the data

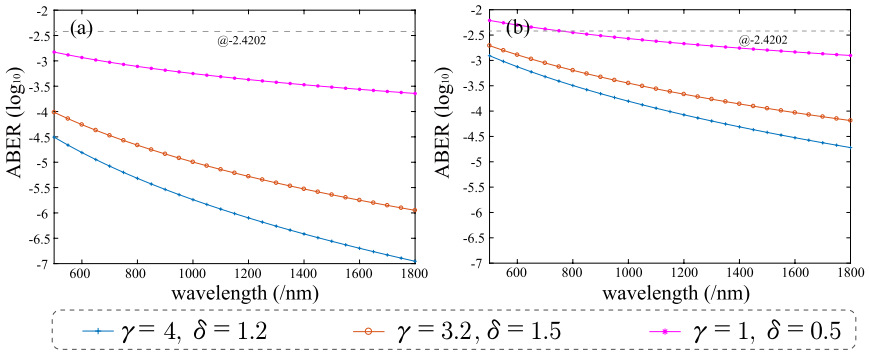

FIGURE 9. ABER as a function of optical wavelength λ for MPSK. @-2.4202 denotes 3.8×10^{-3} ABER, $M = 4$, $\eta_1 = \eta_2 = 0.9$, $\varepsilon = 0.5$, $\xi = 1.0 \times 10^5$, $G = 200$, $T = 300$ *K*, $R = 50\ \Omega$, $B = 4$ *GHz*, *symbol rate* $= 2$ *GB/s*, $i_{d1} = i_{d2} = 1.0 \times 10^{-9}$ *nA*, $I_l = 3.9794$ *dBm*. (a) and (b) represent $I_{soptimal} = -30$ *dBm*, -35 *dBm*, respectively.

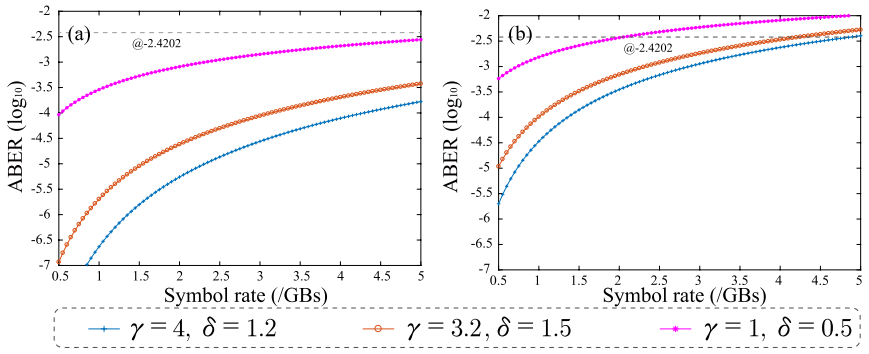

FIGURE 10. ABER as a function of symbol rate for MPSK. @-2.4202 denotes 3.8×10^{-3} ABER, $M = 4$, $\eta_1 = \eta_2 = 0.9$, $\lambda = 1550$ *nm*, $\varepsilon = 0.5$, $\xi = 1.0 \times 10^5$, $G = 200$, $T = 300$ *K*, $R = 50\ \Omega$, $i_{d1} = i_{d2} = 1.0 \times 10^{-9}$ *nA*, $I_l = 3.9794$ *dBm*. (a) and (b) represent $I_{soptimal} = -30$ *dBm* and -35 *dBm*, respectively.

transmission rate. If $\gamma = 3.2, \delta = 1.5, I_l = -35\ dBm$, the ABER at the 0.5 GB/s (1 Gb/s) is 5 orders of magnitude lower than 2.5 GB/s (5 Gb/s), as shown in Fig. 10(b). These phenomena are explained in our previous high-speed communication experiments [12].

Based on the above parameter analysis, we can assume that the splitting ratio is 0.5, and the LO optical power is about -10 *dBm* or less in actual operation [12], [13]. At this point, the effects of dark current noise and thermal noise are negligible, that is,

$$I_{d1} \approx 0, \quad I_{d2} \approx 0, \quad \sigma^2_{thermal-balance} \approx 0, \tag{37}$$

Substituting the (37) into the (34), there is

$$P_{ABER} = \int_0^{\infty} \frac{2}{\log_2 M} \frac{\delta}{\sqrt{2\pi}} \frac{SNR_{optimal}}{SNR(SNR_{optimal} - SNR)} \times \exp\left\{-\frac{1}{2}\left[\gamma + \delta \ln\left(\frac{SNR}{SNR_{optimal} - SNR}\right)\right]^2\right\} \times Q\left(\sqrt{(2\log_2 M)SNR}\sin\frac{\pi}{M}\right) dSNR. \tag{38}$$

We found that (35) can be simplified to $SNR = 2\eta I_s / h\nu B$. If the $\rho = \eta / h\nu B$ is defined as the performance parameter of balanced detector, we can derive the optimal SNR of the fiber-coupling FSO communication system, i.e., $SNR_{optimal} = 2\rho I_{soptimal}$. Where the (38) is a ABER expression about SNR. According to [34], [35], the (38) can be can be approximated as

$$P_{ABER} \approx \sum_{i=1}^{m} w_i \frac{2}{\sqrt{\pi}\log_2 M} \times Q\left(\sqrt{\frac{2\log_2 M SNR_{optimal}}{1 + \exp\{\frac{-\sqrt{2}x_i + \gamma}{2\delta}\}}}\sin\frac{\pi}{M}\right). \tag{39}$$

Equation (39) is a closed ABER expression, where m is the order of approximation, x_i are the zeros of the i^{th}-order Hermite polynomial, and w_i is weight factors for the i^{th}-order approximation, respectively [34, Eqs. (1) and (2)]. To further discuss the performance advantages of MPSK, the relationships between BER and SNR of 4PSK and 4PAM were described in Fig. 11. The ABER of 4PSK is less than 4PAM at the same atmospheric conditions, this effect is becoming more and more obvious as the SNR increases, especially after 20 dB SNR. It shows that the ABER performance of 4PSK is superior to 4PAM at the same channel. Moreover, in 4PSK, under $\gamma = 0.5$, $\delta = 1.0$, $\overline{\sigma_{I_s}^2} = 1.2242$, the ABER of 4PSK is less than the 7% FEC limit of 3.8×10^{-3} when the SNR is 28 dB. And yet 38 dB SNR is required to achieve this goal at $\gamma = 2.8$, $\delta = 0.56$, $\overline{\sigma_{I_s}^2} = 5.2441$. If the ABER is required

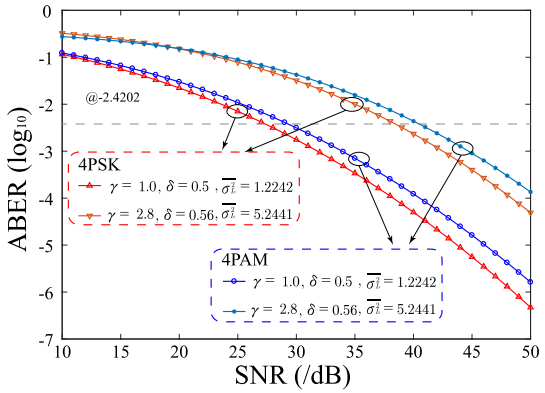

FIGURE 11. ABER as a function of SNR for MPSK and MPAM under different Johnson S_B turbulence channel. @-2.4202 denotes 3.8×10^{-3} ABER, $M = 4$.

to be lower than 10^{-6} at $\gamma = 0.5$, $\delta = 1.0$, $\overline{\sigma_{I_s}^2} = 1.2242$, the SNR at this time should maintain at least 48 *dB* or more. It indicates that the ABER seriously deteriorates with the enhancement of atmospheric turbulence strength, which shall need high SNR to achieve communication. Based on such numerical experimental analysis, we can utilize adaptive optical techniques to reduce the normalized fluctuation variance and use the tracking server system to improve the coupling efficiency for ameliorating the communication performance of the fiber-coupling FSO communication system [36].

V. CONCLUSION

In this paper, by utilizing the fiber-coupling system to receive the free-space optical signal, the ABER performance expression for MPSK communication based on the balanced detector with fiber was illustrated for the first time. Firstly, the Johnson S_B channel fading PDF was first experimentally demonstrated, which described the statistical characteristics of fading when the free-space light is coupled into the SMF after through the atmospheric turbulence. Secondly, an ABER expression was established by combining the photon characteristics of the balanced detector with fiber which base on Johnson S_B. We knew, through numerical simulation, the system is affected by the received optical field, the coupling efficiency of the SMF, and the optical power normalized fluctuation variance which is caused by atmospheric turbulence. In the event that the quantum efficiencies of the two PIN photodetector are equal and the splitting ratio performance is optimal, the excess noise can be eliminated, and the ABER can also be reduced. The performance of ABER is poorer with the deterioration of channel quality, i.e., the normalized fluctuation variance becomes larger, which makes free-space optical signal difficult to be coupled into the SMF. Furthermore, we noted that the communication quality can be ameliorated by adjusting these parameters, i.e, increasing the system bandwidth, selecting the appropriate modulation order, optical wavelength, and data transmission rate, improving the received power of the fiber, increasing the gain of the balanced detector, and controlling the temperature. Finally, in the case where the LO optical power is much larger than the MPSK optical power, the ABER-SNR analytical expression was deduced. This mathematical model described the relationship between the required SNR to successfully communicate in different atmospheric channel scenes. if the normalized fluctuation variance is 1.2242 and the ABER is required to be lower than 10^{-6}, the numerical experimental results manifested that the SNR at this time should maintain at least 48 dB or more. Meanwhile, by numerically analyzing the performance of ABER-SNR, we can also conclude that the communication performance of MPSK is superior to the MPAM in the same channel. In a word, all the presented models can provide parameter reference for the design of fiber-coupling FSO communication system and theoretical support for experiments.

REFERENCES

[1] H. Singh and A. S. Sappal, "Analytic and simulative comparison of turbulent FSO system with different modulation techniques," *Opt. Laser Technol.*, vol. 114, pp. 49–59, Jun. 2019.
[2] H. Singh and A. S. Sappal, "Moment-based approach for statistical and simulative analysis of turbulent atmospheric channels in FSO communication," *IEEE Access*, vol. 7, pp. 11296–11317, 2019.
[3] H. Yao, X. Ni, C. Chen, B. Li, X. Zhang, Y. Liu, S. Tong, Z. Liu, and H. Jiang, "Performance of M-PAM FSO communication systems in atmospheric turbulence based on APD detector," *Opt. Express*, vol. 26, no. 18, pp. 23819–23830, Sep. 2018.
[4] H. Yao, X. Ni, Z. Liu, C. Chen, B. Li, X. Zhang, S. Tong, and H. Jiang, "Experimental demonstration of 4-PAM for high-speed indoor free-space OW communication based on cascade FIR-LMS adaptive equalizer," *Opt. Commun.*, vol. 426, pp. 490–496, Nov. 2018.
[5] J. Li, J. Q. Liu, and D. P. Taylor, "Optical communication using subcarrier PSK intensity modulation through atmospheric turbulence channels," *IEEE Trans. Commun.*, vol. 55, no. 8, pp. 1598–1606, Aug. 2007.
[6] X. Song, F. Yang, J. Cheng, and M.-S. Alouni, "Subcarrier MPSK/MDPSK modulated optical wireless communications in lognormal turbulence," in *Proc. Wireless Commun. Netw. Conf.*, Mar. 2015, pp. 41–45.
[7] P. Conroy, J. Surof, J. Poliak, and R. M. Calvo, "Demonstration of 40 GBaud intradyne transmission through worst-case atmospheric turbulence conditions for geostationary satellite uplink," *Appl. Opt.*, vol. 57, no. 18, pp. 5095–5101, Jun. 2018.
[8] J. Surof, J. Poliak, and R. M. Calvo, "Demonstration of intradyne BPSK optical free-space transmission in representative atmospheric turbulence conditions for geostationary uplink channel," *Opt. Lett.*, vol. 42, no. 11, pp. 2173–2176, Jun. 2017.
[9] Z. Qu and I. B. Djordjevic, "500 Gb/s free-space optical transmission over strong atmospheric turbulence channels," *Opt. Lett.*, vol. 41, no. 14, pp. 3285–3288, Jul. 2016.
[10] G.-W. Lu, T. Sakamoto, A. Chiba, T. Kawanishi, T. Miyazaki, K. Higuma, M. Sudo, and J. Ichikawa, "Reconfigurable multilevel transmitter using monolithically integrated quad Mach–Zehnder IQ modulator for optical 16-QAM and 8-PSK generation," *Opt. Express*, vol. 19, no. 6, pp. 5596–5601, Mar. 2011.
[11] X. Feng, Z. Wu, T. Wang, P. Zhang, X. Li, H. Jiang, Y. Su, H. He, X. Wang, and S. Gao, "Experimental demonstration of bidirectional up to 40 Gbit/s QPSK coherent free-space optical communication link over ~ 1 km," *Opt. Commun.*, vol. 410, pp. 674–679, Mar. 2018.
[12] X. Liu, T. Wang, X. Zhang, J. Chen, P. Lin, H. Yao, J. Zhan, Q. Fu, J. Yang, and H. Jiang, "128 Gbit/s free-space laser transmission performance in a simulated atmosphere channel with adjusted turbulence," *IEEE Photon. J.*, vol. 10, no. 2, Apr. 2018, Art. no. 7902310.
[13] X. Feng, Z. Wu, T. Wang, H. Jiang, Y. Su, H. Jiang, and S. Gao, "120 Gbit/s high-speed WDM-QPSK free-space optical transmission through 1 km atmospheric channel," *Electron. Lett.*, vol. 54, no. 18, pp. 1082–1084, Sep. 2018.
[14] W. O. Popoola and Z. Ghassemlooy, "BPSK subcarrier intensity modulated free-space optical communications in atmospheric turbulence," *J. Lightw. Technol.*, vol. 27, no. 8, pp. 967–973, Apr. 15, 2009.

[15] H. E. Nistazakis, A. N. Stassinakis, H. G. Sandalidis, and G. S. Tombras, "QAM and PSK OFDM RoFSO over M-turbulence induced fading channels," *IEEE Photon. J.*, vol. 7, no. 1, Feb. 2015, Art. no. 7900411.

[16] K. A. Balaji and K. Prabu, "BER analysis of relay assisted PSK with OFDM ROFSO system over Malaga distribution including pointing errors under various weather conditions," *Opt. Commun.*, vol. 426, pp. 187–193, Nov. 2018.

[17] W. Gappmair and H. E. Nistazakis, "Subcarrier PSK performance in terrestrial FSO links impaired by Gamma-Gamma fading, pointing errors, and phase noise," *J. Lightw. Technol.*, vol. 35, no. 9, pp. 1624–1632, May 1, 2017.

[18] K. Kiasaleh, "Performance of coherent DPSK free-space optical communication systems in K-distributed turbulence," *IEEE Trans. Commun.*, vol. 54, no. 4, pp. 604–607, Apr. 2006.

[19] K. Li, J. Ma, L. Tan, S. Yu, and C. Zhai, "Performance analysis of fiber-based free-space optical communications with coherent detection spatial diversity," *Appl. Opt.*, vol. 55, no. 17, pp. 4649–4656, 2016.

[20] H. Hemmati, *Deep Space Optical Communications*. Hoboken, NJ, USA: Wiley, 2006.

[21] Y.-H. Wang and I. Lyubomirsky, "Balanced detection schemes for optical duobinary communication systems," *J. Lightw. Technol.*, vol. 29, no. 12, pp. 1739–1745, Jun. 15, 2011.

[22] K. Kikuchi, "Fundamentals of coherent optical fiber communications," *J. Lightw. Technol.*, vol. 34, no. 1, pp. 157–179, Jun. 1, 2016.

[23] A. Leven, N. Kaneda, U.-K. Koc, and Y.-K. Chen, "Coherent receivers for practical optical communication systems," in *Proc. OFC/NFOEC Conf. Opt. Fiber Commun. Nat. Fiber Optic Eng. Conf.*, Mar. 2007, pp. 1–3.

[24] L. C. Andrews and R. L. Phillips, *Laser Beam Propagation Through Random Media*, 2nd ed. Bellingham, WA, USA: SPIE, 2005.

[25] C. Chen and H. Yang, "Shared secret key generation from signal fading in a turbulent optical wireless channel using common-transverse-spatial-mode coupling," *Opt. Express*, vol. 26, no. 13, pp. 16422–16441, Jun. 2018.

[26] M. F. Mesiya, *Contemporary Communication Systems*. New York, NY, USA: McGraw-Hill, 2013. [Online]. Available: http://gen.lib.rus.ec/book/index.php?md5=490055a3d502482e6e78304ac18d19c1

[27] B. C. Levy, *Principles of Signal Detection and Parameter Estimation*, 1st ed. New York, NY, USA: Springer, 2008.

[28] Y. Painchaud, M. Poulin, M. Morin, and M. Têtu, "Performance of balanced detection in a coherent receiver," *Opt. Express*, vol. 17, no. 5, pp. 3659–3672, Mar. 2009.

[29] B. L. Schumaker, "Noise in homodyne detection," *Opt. Lett.*, vol. 9, no. 5, pp. 189–191, May 1984.

[30] H. P. Yuen and V. W. S. Chan, "Noise in homodyne and heterodyne detection," *Opt. Lett.*, vol. 8, no. 3, pp. 177–179, 1983.

[31] L. A. Coldren, S. W. Corzine, and M. L. Mashanovitch, *Diode Lasers and Photonic Integrated Circuits*. Hoboken, NJ, USA: Wiley, 1995.

[32] A. Yariv and P. Yeh, *Photonics: Optical Electronics in Modern Communications* (The Oxford Series in Electrical and Computer Engineering), 6th ed. New York, NY, USA: Oxford Univ. Press, 2006.

[33] A. Leven, F. Vacondio, L. Schmalen, S. ten Brink, and W. Idler, "Estimation of soft FEC performance in optical transmission experiments," *IEEE Photon. Technol. Lett.*, vol. 23, no. 20, pp. 1547–1549, Oct. 15, 2011.

[34] Q. Liu and D. A. Pierce, "A note on gauss-Hermite quadrature," *Biometrika*, vol. 81, no. 3, pp. 624–629, Aug. 1994.

[35] Q. Shi and Y. Karasawa, "An accurate and efficient approximation to the Gaussian Q-function and its applications in performance analysis in nakagami-m fading," *IEEE Commun. Lett.*, vol. 15, no. 5, pp. 479–481, May 2011.

[36] A. Mansour, R. Mesleh, and M. Abaza, "New challenges in wireless and free space optical communications," *Opt. Lasers Eng.*, vol. 89, pp. 95–108, Feb. 2017.

HAIFENG YAO received the B.S. degree from the School of Optoelectronic Engineering Technology, Changchun University of Science and Technology, Changchun, China, in 2017, where he is currently pursuing the Ph.D. degree. His research interests include free-space optical communications, design of communication circuit, modeling and simulation of light propagation in complex environments, and the field of coherent detection.

XIAOLONG NI received the Ph.D. degree from the Department of Electronic Information, Changchun University of Science and Technology, Changchun, China, where he is currently a Lecturer. His current research interests include free-space communications, beam propagation in atmospheric turbulence, and adaptive optics.

CHUNYI CHEN is currently a Professor with the Changchun University of Science and Technology. His research interests include beam propagation in atmospheric turbulence, free-space optical communications, and modeling and simulation of light propagation in complex environments. He has reviewed journal manuscripts for the OSA.

BO LI received the B.S. degree from the School of Optoelectronic Engineering Technology, Changchun University of Science and Technology, Changchun, China, in 2017, where he is currently pursuing the Ph.D. degree. His research interests include free-space optical communications and design of optical systems.

XIANGLIAN FENG received the B.S. degree from Zhejiang University, China, in 2016, where she is currently pursuing the Ph.D. degree. Her research interests include free-space optical communications and coherent communication.

XIANZHU LIU received the Ph.D. degree from the Department of Electronic Information, Changchun University of Science and Technology, Changchun, China, where he is currently a Lecturer. His current research interest includes free-space communications.

ZHI LIU received the Ph.D. degree from the Department of Electronic Information, Changchun University of Science and Technology, Changchun, China, where he is currently a Professor. His current research interest includes free-space communications.

SHOUFENG TONG received the Ph.D. degree from the Department of Electronic Information, Changchun Institute of Optics, Fine Mechanics and Physics, Chinese Academy of Sciences, Jilin, China. He is currently a Professor with the Changchun University of Science and Technology. He currently specializes in optical engineering and is the Provincial Key Leader of a team responsible for teaching in that field. His current research interests include laser communication and telemetry remote sensing technology. He was a recipient of the Yangtze River Scholar Award and successfully won the 2014 National Talent Project, in 2014.

HUILIN JIANG is currently an Academician of the Chinese Academy of Engineering Information and Electronic Engineering. He is also a Professor with the Changchun University of Science and Technology. His research interests include beam propagation in atmospheric turbulence, free-space optical communications, and optical system design. He is hailed as the Outstanding Representative of the third generation of China's optical industry. He has presided over the national 863 key project and 995 high-tech. More than 20 projects, including the 973 major basic research project and the National Natural Science Foundation project, have made outstanding contributions to China. In addition, he has served as the Vice Chairman of the China Armed Forces Association, an Executive Director of the Chinese Optical Society, an Executive Director of the first council of the China Optical Engineering Society, a Deputy Director of the National Steering Committee for Weapons in Colleges and Universities, a member of the International Society of Optical Engineering (SPIE), a Deputy Director of the Academic Committee of the State Key Laboratory of Applied Optics, a Deputy Director of the Academic Committee of the National Key Laboratory of High Power Semiconductor Laser, Changchun University of Science and Technology, a member of the Academic Committee of the Key Laboratory of Advanced Manufacturing Technology for Optical Systems, Chinese Academy of Sciences, and a member of the Academic Committee of the Key Laboratory of Computational Optics.